

## Retrieval of monthly maximum and minimum air temperature using MODIS aqua land surface temperature data over the United Arab Emirates

Abduldaem S. Alqasemi , Mohamed E. Hereher , Ayad M. Fadhil Al-Quraishi , Hakim Saibi , Ala Aldahan & Abdelgadir Abuelgasim

To cite this article: Abduldaem S. Alqasemi , Mohamed E. Hereher , Ayad M. Fadhil Al-Quraishi , Hakim Saibi , Ala Aldahan & Abdelgadir Abuelgasim (2020): Retrieval of monthly maximum and minimum air temperature using MODIS aqua land surface temperature data over the United Arab Emirates, Geocarto International, DOI: [10.1080/10106049.2020.1837261](https://doi.org/10.1080/10106049.2020.1837261)

To link to this article: <https://doi.org/10.1080/10106049.2020.1837261>



© 2020 The Author(s). Published by Informa UK Limited, trading as Taylor & Francis Group.



Published online: 28 Oct 2020.



Submit your article to this journal [↗](#)



Article views: 159








View related articles [↗](#)



View Crossmark data [↗](#)

# Retrieval of monthly maximum and minimum air temperature using MODIS aqua land surface temperature data over the United Arab Emirates

Abduldaem S. Alqasemi<sup>a</sup> , Mohamed E. Hereher<sup>b</sup> , Ayad M. Fadhil Al-Quraishi<sup>c\*</sup> , Hakim Saibi<sup>d</sup> , Ala Aldahan<sup>d</sup> and Abdelgadir Abuelgasim<sup>a</sup> 

<sup>a</sup>Geography and Urban Sustainability, College of Humanities & Social Science, United Arab Emirates University, Al-Ain, UAE; <sup>b</sup>Geography Department, College of Arts and Social Sciences, Sultan Qaboos University, Muscat, Oman; <sup>c</sup>Department of Environmental Engineering, College of Engineering, Knowledge University, Erbil, Iraq; <sup>d</sup>Geology Department, College of Science, United Arab Emirates University, Al-Ain, UAE

## ABSTRACT

Spatially distributed air temperature ( $T_a$ ) data are essential for environmental studies.  $T_a$  data are collected from meteorological stations of sparse distribution. This problem can be overcome by using remotely sensed datasets at different scales. This study used land-based temperature measurements and satellite data for estimating  $T_a$  distribution over the United Arab Emirates. Land-based  $T_a$  data from 11 weather stations during 2003 to 2019 were used with MODIS Aqua LST for both daytime (LSTd) and nighttime (LSTn) data. The results indicate a significant correlation between LST and  $T_a$  with regression coefficients  $R^2 > 0.94/0.96$  and Root Mean Square Error about  $1.75/0.97^\circ\text{C}$  of LSTd/ $T_{\max}$  and LSTn/ $T_{\min}$ , respectively. Large variability was observed between the daytime and nighttime mean temperature distribution indicating the importance of MODIS LST as a proxy for  $T_a$ . These countrywide  $T_a$  grids provide vital tools for the planning of environmental and economic developments in the era of global climate change.

## ARTICLE HISTORY

Received 27 June 2020  
Accepted 29 September 2020

## KEYWORDS

Air temperature;  
meteorological station data;  
land surface temperature;  
MODIS; UAE;  
linear regression

## 1. Introduction

Meteorological data such as air temperature ( $T_a$ ) represent essential information for the economic development of the society for a variety of predictions ranging from precipitation trends, storms, heat waves, tourism, among other areas.  $T_a$  is important as it is commonly used in climate modelling, global change predictions, and modelling the exchange processes between the atmosphere, biosphere, and hydrosphere. Accurate determination of its spatial, temporal distribution and variability is vital for applications in the fields of

**CONTACT** Abduldaem S. Alqasemi  [a.alqasemi@uaeu.ac.ae](mailto:a.alqasemi@uaeu.ac.ae)

\*Additional affiliation: Surveying and Geomatics Engineering Department, Faculty of Engineering, Tishk International University, Erbil 44001, Kurdistan Region, Iraq.

© 2020 The Author(s). Published by Informa UK Limited, trading as Taylor & Francis Group.

This is an Open Access article distributed under the terms of the Creative Commons Attribution-NonCommercial-NoDerivatives License (<http://creativecommons.org/licenses/by-nc-nd/4.0/>), which permits non-commercial re-use, distribution, and reproduction in any medium, provided the original work is properly cited, and is not altered, transformed, or built upon in any way.

hydrology, agriculture, environmental and ecological assessments, climate change, and related societal development (IPCC 2017).

*Ta* data are usually collected by measurements at meteorological stations over both land and water surfaces. The measurements provide the benefit of high temporal resolution and accuracy. However, these data being point measurements do not reflect *Ta* spatial distribution and missing variability may not be observed (Otgonbayar et al. 2019). These limitations can bias *Ta* spatial distribution estimation, especially in the advanced spatial interpolations (Huang et al. 2015).

Moreover, changes in topography (elevation), and geometry of station location also affects the interpolation accuracy, specifically in elevated areas (Vancutsem et al. 2010; Shah et al. 2012; Zhu et al. 2013; Huang et al. 2015; Noi et al. 2016). A large part of these discrepancies from *in-situ* measurements of *Ta* have been overcome by using remotely sensed thermal infrared radiance that can be used to derive land surface temperature (LST). The LST is described as a radiating temperature of the land surface, which is observed by satellite sensors (Fadhil 2011; Kloog et al. 2014). LST can only be derived from infrared (IR) channels for clear sky conditions as most of the clouds are opaque to IR energy, which is emitted from the surface. Although LST is not directly driven by solar radiance (Xu et al. 2012), it has a strong correlation with *Ta*, and it is considered one of the essential sources of data for *Ta* retrieval over a region or large area (Jones et al. 2004; Chen et al. 2016; Hereher 2019; Phan et al. 2019; Hereher and El Kenawy 2020).

The combination of meteorological stations data with the remotely sensed dataset assists the making of mesoscale maps for the distribution of LST by upscaling point data from meteorological stations (Shah et al. 2012; Huang et al. 2015). Remote sensing data offer a good solution to overcome the limitations of the interpolation methods. The capability to get both high temporal and spatial resolutions makes LST data an essential benefit of satellite observations over conventional climatic datasets (Kloog et al. 2014; Serra et al. 2020).

Many satellite sensors provide thermal data to retrieve LST, such as the Landsat TM/ETM+/TIRS, Advanced Spaceborne Thermal Emission and Reflection Radiometer (ASTER), Advanced Very High-Resolution Radiometer (AVHRR), and the Moderate Resolution Imaging Spectroradiometer (MODIS). Among these satellite data, Landsat and ASTER have a coarse temporal as well as spatial resolution of 16 days and 90–100 m, respectively (Phan et al. 2019). Thus, for *Ta* estimation, MODIS LST is considered a suitable source of data, and it is widely used in different applications due to its free availability, high thermal resolution, and can be obtained easily (Hereher 2017; Zhou et al. 2017; Meyer et al. 2019; Hereher and El Kenawy 2020).

As far as we know, no research has been conducted to estimate *Ta* over the UAE. Therefore, the primary objectives of this research study was to derive the components of two *Ta* (max and min) from LST using MODIS data over the UAE.

## 2. Data and methods

### 2.1. The study area

The study area is the United Arab Emirates located between latitudes 22°–26° N and longitudes 51°–56° E (Figure 1). It has an approximate area of about 83,600 km<sup>2</sup>. It is located on the Arabian Peninsula, one of the driest places on earth with an annual average precipitation of 100 mm that may reach up to 300 mm in the mountains and less than 50 mm in the desert (Murad and Aldahan 2019). The desert occupies about 80% of the UAE land area. Although the annual average air temperature is around 28 °C, it is much

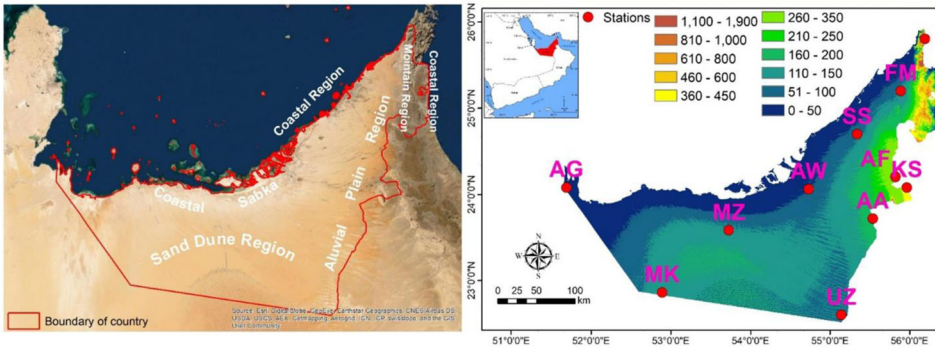


**Figure 1.** Topography (m.a.s.l.), major geomorphic regions, and the spatial distribution of meteorological stations.

warmer (up to 50 °C) in summer (June–August) and cools down to 10 °C in winter (December–February). The average number of sunny days is about 300, and dust storms occur within the range between 5 and 60 hours per year depending on location, with the highest events near to the desert areas and lowest along the mountains (Barbulescu and Nazzal 2020).

## 2.2. Data

### 2.2.1. Topography data

The study area is almost flat and homogeneous in the western and coastal parts, with most topographic undulations related to the sand dunes field. In the northeastern part of the UAE, there are mountain ranges with a maximum altitude up to 1900 m. The spatial distribution of the terrain topography is shown on Figure 1, as estimated from the Shuttle Radar Topography Mission (SRTM).

### 2.2.2. Air temperature data

Monthly mean  $T_{max}$  and  $T_{min}$  (°C) data for the period 2003–2019 were obtained from 11 automatic meteorological stations from different parts of the country collected by the National Center of Meteorology and Seismology (NCMS) (Figure 1). All the stations provided full records without gaps or missing values over the entire period. The distribution of the meteorological stations that were used here covers the mountainous area at an elevation of approximately 1739 m (Jabal Jais station), one coastal area (Al Ghweifat station), and the remaining nine stations are dispersed in the desert and bare land. The available weather stations are mostly below an altitude of 450 m above sea level.

### 2.2.3. Modis LST data

The MODIS instrument is aboard the NASA Earth Observing System Aqua and Terra satellites. In December 1999, the Terra satellite was launched, while the Aqua was launched in May 2002. Worldwide coverage is given by their orbital parameters in 1–2 days, and provide LST four times daily, including daytime (LSTd) and nighttime (LSTn). At about 10:30 am, Terra descends past the equator, and at about 10:30 pm, it ascends past the equator. In comparison, Aqua passes the equator at about 1:30 am and 1:30 pm in opposite directions. Every 24 hours, at the same time, both satellites pass above the same location on Earth (<https://modis.gsfc.nasa.gov/data/>).

There are two thermal infrared bands used to derive the MODIS LST, i.e. 31 (10.78–11.28  $\mu\text{m}$ ) and 32 (11.77–12.27  $\mu\text{m}$ ) using the split-window algorithm (Wan et al. 2002). The accuracy is 1K in most of the cases under the clear sky, as per the results of ground validation of these LST products. This level of accuracy can achieve requirements for the accuracy of most LST modelling applications (Wang et al. 2008). From mid-2002 (Aqua) and early 2000 (Terra), MODIS LST data has gained significant attention and is widely used for the estimation of  $T_a$ . It also has shown its suitability as a proxy for  $T_a$  in neighbouring countries such as Egypt (El Kenawy, Hereher, et al. 2019; El Kenawy, Lopez-Moreno, et al. 2019; Hereher and El Kenawy 2020), Iran (Janatian et al. 2017) and Oman (Hereher 2019). These previous results serve as a verification of the precision of MODIS products, which reach the requirements of  $T_a$  estimation.

The LSTd and LSTn adopted here were extracted from the Aqua 8-day LST and Emissivity MODIS product Version-6. The LST product, such as MYD11A2, covers the time period 1 January 2003 to 31 December 2019. The Land Processes Distributed Active Archive Center of NASA (LP DAAC) provided all products in the two MODIS tiles of granules with horizontal (h) and vertical (v) title numbers h22v06 and h23v06 (<https://lpdaac.usgs.gov/>). Brightness value (16-bit) is represented by each image, in Hierarchical Data Format (HDF), and at a Sinusoidal Projection, in relation to the LST in Kelvin. The images are 1 km spatial resolution and contain layers of LSTd and LSTn.

Although daily data of MODIS Aqua for the product MYD11A1 is available from January 2003, we use here the composite product MYD11A2. The reason for selecting 8-day data is better data coverage (i.e. no gaps in data except persistent cloud coverage). In other words, due to correction of cloud contamination, the available data is more continuous, and therefore, the quantity of available data points for comparison for 8-day average is remarkably less than the available daily average dataset (Hengl et al. 2012; Shah et al. 2013; Singh et al. 2019). The accuracy of this product (MYD11A2), according to NASA's Goddard Space Flight Center, was reported better when compared to 1K in clear sky conditions (<https://modis-land.gsfc.nasa.gov/>). Thus, for the entire UAE, a set of LST 8-day composite products (MYD11A2) was acquired.

MODIS LST data Version-6 (or collection-6) was used because of significant changes, and improvement that were made for this version (Wan 2014). In these improvements, the most critical changes of version-6 in comparison to the previous version is removing cloud contaminated LST pixels. The accuracy of the LST version-6 product was reported to be two times better than version-5 (Duan et al. 2018). According to Vancutsem et al. (2010), when selecting the data for a specific area, it is essential to consider the time of overpass. Thus, MODIS Aqua data was selected for the UAE as this sensor overpasses at 1.30 pm and 1.30 am which is closest to  $T_{\text{max}}$  and  $T_{\text{min}}$  measurement time, so the LSTd and LSTn from the satellite measurements could be estimated and compared with the ground weather station recorded  $T_{\text{max}}$  and  $T_{\text{min}}$ .

## 2.3. Methods

### 2.3.1. Pre-processing MODIS LST data

At weather stations, many steps were followed to retrieve the data of LST under clear sky conditions. A total of 1564 MODIS images (MYD11A2, h22v06, and h23v06, Version-6) were collected. The HDF images were projected to WGS1984 UTM Zone 40 N, for the study period, over the UAE, using the nearest neighbour resampling method. The corresponding layers (LSTd and LSTn) were extracted in TIF format. After that, a mosaic of two tiles was created, and the images were clipped using the boundary polygon, which

defines the study area. Finally, LST data were aggregated to a monthly period by averaging the 8-day composite data to obtain monthly average LST<sub>d</sub> and LST<sub>n</sub>, to provide direct comparison to the maximum and minimum monthly average that were used to represent *T<sub>a</sub>* data.

Using batch processing of extract multi-value, MODIS LST data for the pixels were extracted from TIF format MODIS images in which the weather stations are located to points in the ArcGIS program. Using the following equation, all these LST data (DN values) were converted to Celsius temperature:

$$\text{LST } (^{\circ}\text{C}) = a * \text{DN} - 273.15 \quad (1)$$

where  $^{\circ}\text{C}$  is Celsius LST, and  $a$  is scaling factor (0.02) of MODIS LST product, which converts the values of scientific data sets into the real values of LST (Kelvin degree) (Wan et al. 2015).

Next, removing outlier data was performed: if clouds are present on a location (pixel), then MODIS LST products are unavailable for that location (Wan 2008); however, some pixels which are slightly covered by clouds are not removed as the covering is minimal, and the cloud-removing mask algorithm cannot detect those (Noi et al. 2017). Hence, all unrealistic values of LST data, which have values higher than  $100^{\circ}\text{C}$  or less than  $-50^{\circ}\text{C}$  or any value beyond the valid range, were marked as no data and ignored in the procedure to provide a seamless dataset. Consequently, only clear, reliable pixels, and good quality data were used according to the Quality Assessment (QA) layer. All images for each month were placed together to make a single file for each daytime and nighttime. The monthly average for LST<sub>d</sub> and LST<sub>n</sub> was determined using the Cell Statistics model for all the images between 2003 – 2019. Finally, the Extract Multi Value model was used to derive LST<sub>d</sub> and LST<sub>n</sub> from a single pixel where weather stations are located and those values were converted to Excel Spreadsheets before matching them with the corresponding  $T_{\text{max}}$  and  $T_{\text{min}}$ , derived from eleven stations. For the processing, analyzing, displaying, and quality control of the MODIS data, ESRI ArcGIS<sup>TM</sup> 10.4 software was used.

### 2.3.2. Estimation of air temperature using MODIS LST data

Numerous methods have been developed and applied for *T<sub>a</sub>* estimation from MODIS LST data. Benali et al. (2012) and Noi et al. (2016) point out there are three popular methods: statistical, temperature-vegetation index (TVX), and energy-balance modelling. Energy-balance approaches, the sum of incoming anthropogenic heat fluxes and net radiation, are considered similar to the sum of the surface's sensible and latent heat fluxes. Energy-balance approaches, however, require many parameters, which are mostly not directly provided by remote sensing. This is the main disadvantage of energy-balance methods (Mostovoy et al. 2006; Benali et al. 2012; Liu et al. 2019).

On the other hand, only satellite data is required in the TVX and the statistical method, which is easily accessible and is ordinarily available with thermal data (Misslin et al. 2018). One drawback to the TVX method is that performance depends upon the negative correlation among the normalized difference vegetation index (NDVI) and LST, and there is a high variation in NDVI with different satellite sensors. However, this method is not satisfying in some cases because of the supposition that it frequently does not fit to the effect of the reality and seasonality, scarce of vegetation cover throughout the arid environment, soil moisture, or land cover type (Stisen et al. 2007; Janatian et al. 2017; Yang et al. 2017). Therefore, the statistical method is a suitable and straightforward method, which does not present the same limitations.

There is a simple statistical linear regression between  $Ta$  and LST (Vogt et al. 1997; Mostovoy et al. 2006; Hereher 2019; Hereher and El Kenawy 2020) and also advanced approaches in which more than one independent variable are used (Vancutsem et al. 2010; Zhang et al. 2011; Xu et al. 2012; Benali et al. 2012; Noi et al. 2016). The main advantages of the linear regression method is that the regression against station data minimizes systematic regional errors in data of the satellite; they normally provide accurate  $Ta$  estimation within the spatial and temporal frame they were obtained, and they are easier to operate. Thus, simple linear regression is the most intuitive and widely used  $Ta$  estimation method (Stisen et al. 2007; Janatian et al. 2017). However, the statistical methods normally perform well in the spatial and temporal domains, they still require large amounts of data to train the algorithms, especially for the advanced approaches, and have restricted generalization (Stisen et al. 2007).

The criteria of combining data retrieved from satellite and meteorological stations for the same date comprise a one-to-one relationship, linking monthly LSTd and LSTn from satellite data with monthly data obtained from a station ( $T_{max}$  and  $T_{min}$ ). Therefore, for each meteorological station, the LST values (LSTd and LSTn) of the  $1\text{ km}^2$  pixel are extracted, which are superimposed on the station. This process is done for all the existing images data of the study period. The LSTd images values are linked with  $T_{max}$ , and the LSTn images values are linked with  $T_{min}$ . Then the relationship of linear regression is estimated, and for each month, the coefficient of correlation between the monthly LSTd in the satellite image was determined with the  $T_{max}$  of each weather station of the corresponding month. In the same way, the correlation between monthly  $T_{min}$  from the weather stations and monthly LSTn from the satellite data was determined.

The regression equation was generated for the estimation of monthly air temperature maximum ( $Ted$ ) and minimum ( $Ten$ ) from data of LSTd and LSTn for the whole region. The annual daytime, nighttime, and diurnal variation temperature maps were also estimated. The following simple linear regression model was constructed to estimate the  $Ted$  and  $Ten$  from the LST data:

$$Ted = aLSTn + b \quad (2)$$

$$Ten = aLSTn + b \quad (3)$$

where  $a$  and  $b$  are coefficients of regression, which are estimated using ordinary least-squares regression.  $Ted$  and  $Ten$  are the estimated monthly average maximum and minimum air temperature, respectively. The LSTd and LSTn derived from the data of Aqua MODIS can be used as independent variables ( $x$ ), and  $Ta$  ( $T_{max}$  and  $T_{min}$ ) is a dependent variable ( $y$ ). In previous studies, to estimate air temperatures from LST, linear regression was successfully applied (Mostovoy et al. 2006; Kloog et al. 2014; Huang et al. 2015; Hereher 2019; Hereher and El Kenawy 2020). By applying the correlation between the day and night LST data readings versus all records from the 11 stations, the regression model for extracting maximum and minimum air temperatures was determined. Two popular criteria were used to assess the performance of the regression model: the determination coefficient ( $R^2$ ) that was calculated from the  $Ta$  values and LST data from linear regression analysis, and the Root Mean Square Error (RMSE). Calculation of these statistical factors was performed using Excel Microsoft.

### 3. Result and discussion

As shown in Figure 2, a strong linear correlation exists between LST of satellite images and  $Ta$  data of meteorological stations in the study area, for both daytime and nighttime



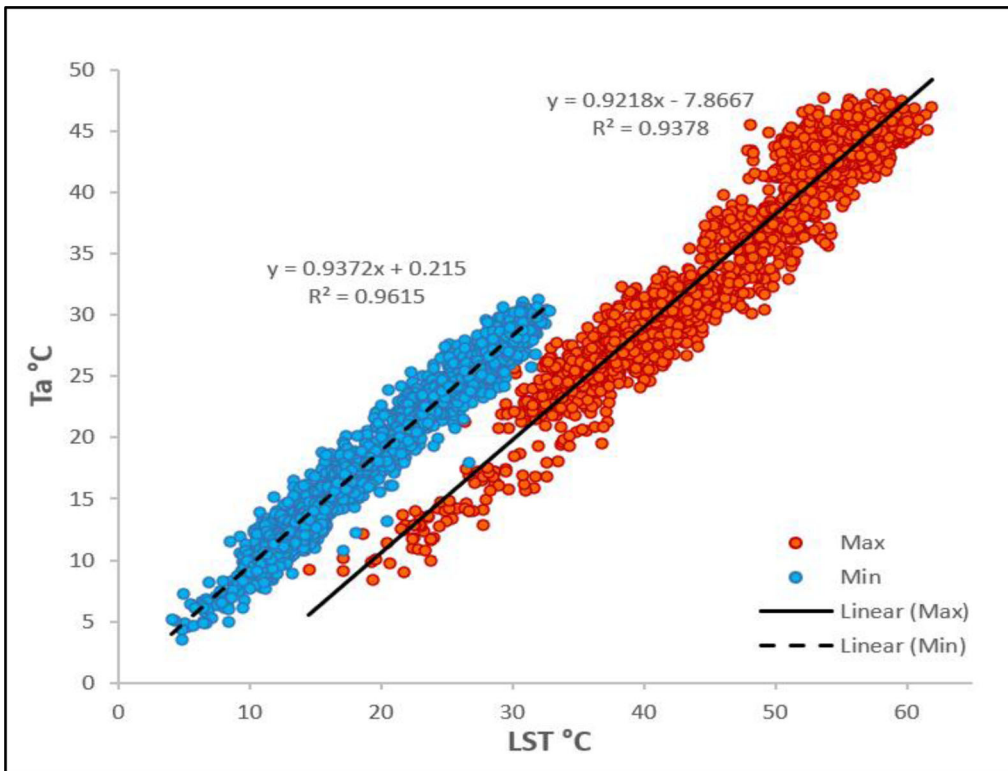


**Figure 2.** The regression correlation between LSTd and  $T_{\max}$  (red) and LSTn and  $T_{\min}$  (blue) for the period 2003–2019 of all stations used in this study.

LST. The determination coefficient ( $R^2$ ) for LSTd and  $T_{\max}$  is 0.94, and 0.96 for the LSTn and  $T_{\min}$  association. The determination coefficient is calculated for the 2003–2019 dataset. For estimation of maximum ( $T_{ed}$ ) and minimum ( $T_{en}$ ) air temperature from the data of MODIS LST, the previous Equations (2) and (3) were used as the following:

$$T_{ed} = 0.9218 \text{ LSTd} - 7.8667 \quad (4)$$

$$T_{en} = 0.9372 \text{ LSTn} + 0.215 \quad (5)$$

Figure 3 shows the scatterplot diagram of the association between the LSTd and  $T_{\max}$  and LSTn and  $T_{\min}$  for the individual studied stations. The coefficients of determination between LSTd and  $T_{\max}$  were very high. The coefficient value between LSTd and  $T_{\max}$  ranges from 0.943 – 0.957, while the LSTn and  $T_{\min}$  correlation were slightly higher at all stations, ranging from 0.963 – 0.985.

From Figures 2 and 3, a significant linear correlation between LST and  $T_a$  was observed. Despite the strong LST and  $T_a$  correlation, their values differ partially. At all stations, the LST and  $T_a$  relationship is slightly better defined by the linear regression during the night than the day. The LSTd is generally higher than  $T_{\max}$ , whereas LSTn is slightly lower and quite close to the  $T_{\min}$ . In other words, during the study period, the difference ( $\text{LSTd} - T_{\max}$ ) is higher than ( $\text{LSTn} - T_{\min}$ ) in all stations. These differences between  $T_a$  and LST increased in the summer season (Jun. to Aug.), in which the daytime is hotter and longer, as shown in Figure 4(a). This trend has also been observed in many other studies (e.g. Zhu et al. 2013; Huang et al. 2015; Hereher 2019; Hereher and El Kenawy 2020). Figure 4 shows that  $T_a$  and LST have seasonal cycles that are similar and



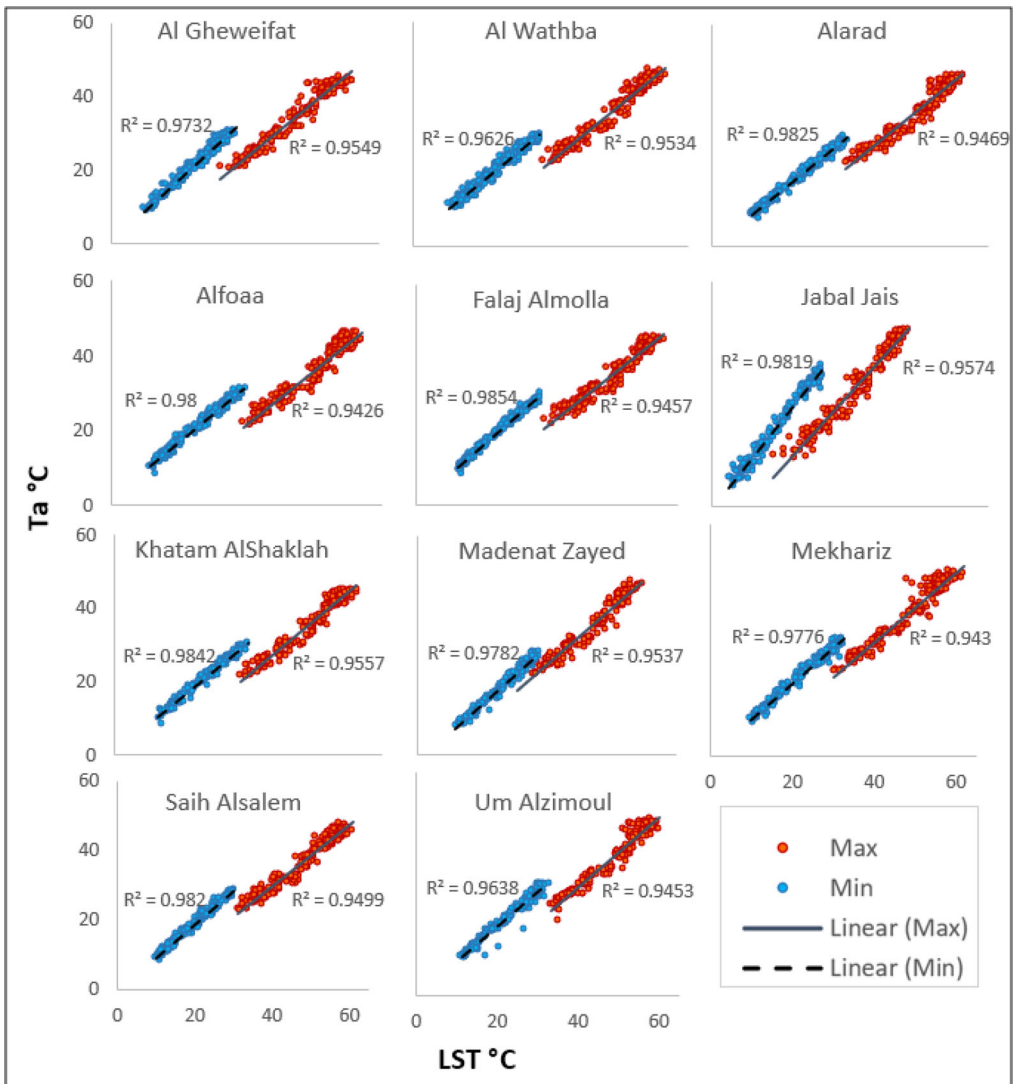


**Figure 3.** Scatterplots diagram showing the association between LSTd and  $T_{\max}$  (red) and LSTn and  $T_{\min}$  (blue) for all stations used in this study. The  $R^2$  value is presented to show the sign of association and the magnitude, (Note the high value of  $R^2$ ).

correlated due to the energy exchange between  $T_a$  and LST that depends on seasonal variation of incoming solar irradiance. This feature relates to the stable stratification of the air parcel due to the radiative cooling at the surface and weakening of turbulence generated by surface friction during the nighttime (Lin et al. 2016). The Earth's surface almost acts as a homogeneous and isothermal surface. Results (Figure 4) show more complex interactions between  $T_a$  and LST during the daytime due to the more turbulent surface and weather conditions that are affected by direct solar illumination and therefore produce a slightly lower model fit (Vancutsem et al. 2010; Kloog et al. 2014). The increase in temperature and concentration of thermal energy at the surface during daytime as the ground absorbs solar radiation causes a partial decoupling of the day LST and  $T_a$  (Lin et al. 2016). This feature makes the LST of the daytime hotter as compared to  $T_a$  (Figure

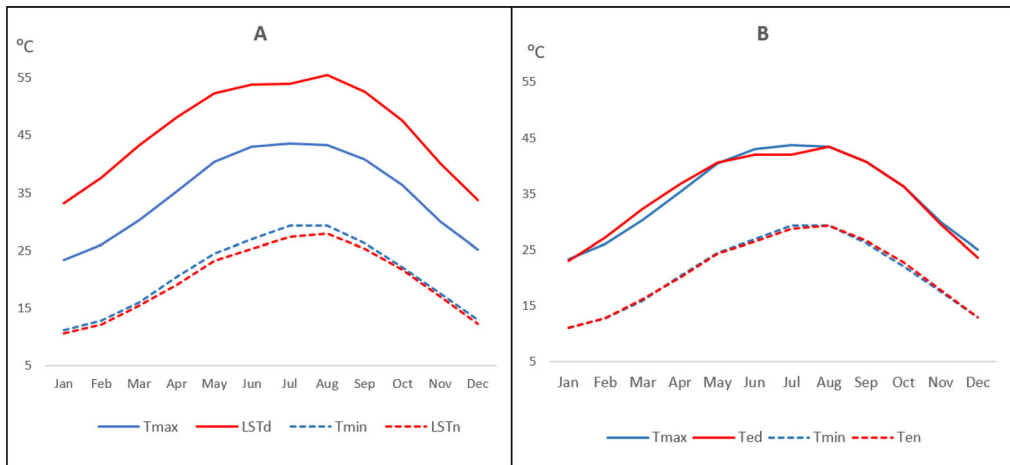


**Figure 4.** The annual cycle of nighttime and daytime temperatures calculated from weather stations (blue) and Aqua LST data (red). (a) Before applying the linear regression method; and (b) is after applying the linear regression method.

4(a)). Also, due to the sunlight and shade effects in pixels during the daytime, a more significant angular anisotropy effect is expected for LST of daytime as compared to the LST of nighttime, which similarly explains the slightly lower model fit (Benali et al. 2012; Zheng et al. 2013).

Furthermore, atmospheric water vapor is also a significant component that traps hot land surface long-wave radiations (Zhang et al. 2011). In our study area, the concentration of water vapor in summer is more like other trace greenhouse gases. Water vapor also has a warming effect on both air and land surface, however, in terms of radiative forcing, the warming effect magnitude of the greenhouse gases is different for the land surface and air (Zhang et al. 2011). This additionally explains why the best performance is at nighttime with a minimum RMSE value of 1.49 °C, whereas, at daytime, the difference between LST<sub>d</sub> and T<sub>max</sub> is significant with RMSE of about 10.37 °C. Nevertheless, after applying the linear regression method, a significant reduction in statistical error was observed, with 1.75 °C at daytime and 0.97 °C at nighttime in all the stations. Figures 4(b) and 5 support the utilization of the linear regression method, showing that the estimated air temperature (T<sub>ed</sub> and T<sub>en</sub>) nearly matches the measured air temperature (T<sub>max</sub> and T<sub>min</sub>).

The high statistical confidence of the linear regression between data from satellite images and observed *T<sub>a</sub>* is discussed here. Therefore, by substituting the LST<sub>d</sub> and LST<sub>n</sub> values, they can be used to derive unknown T<sub>max</sub> and T<sub>min</sub> of any area, respectively. Accordingly, and applying Equations (4) and (5), the UAE's derived daytime and nighttime air temperatures monthly average (T<sub>ed</sub> and T<sub>en</sub>, respectively) are shown in Figures 6 and 7. The average annual daytime and nighttime max and min air temperatures and the diurnal temperature range (DTR) are shown in Figure 8.

The UAE's estimated average monthly maximum air temperatures (T<sub>ed</sub>) during the entire study period (2003–2019) indicate spatial variation in daytime air temperature where the interior is hotter than the coastal and mountain areas (Figure 6). Furthermore, there are four major zones of T<sub>ed</sub> variations that maintain positions that is partly related to seasonal changes. A winter season is marked by the December to February with temperature zoning gradually decreasing from the inland towards the coasts. During March to May (spring season), the hotter inner land T<sub>ed</sub> zone expands and dominates the

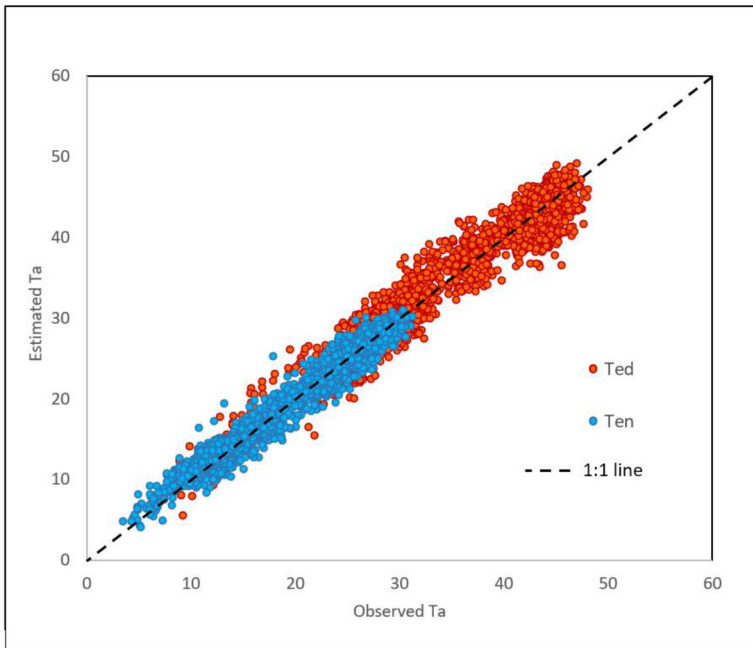


**Figure 5.** A scatter plot for stations' measured  $T_a$  ( $T_{\max}$  and  $T_{\min}$ ) and estimated air temperature (Ted and Ten).

distribution pattern. This trend of expansion continues in the summer months (June–August and even September), leaving only the months of October and November months to initiate cooling and then a return to the winter season pattern in December (Figure 6). The Ted variability of the different zones in the different seasons ranges from  $> 45^\circ\text{C}$  for the hottest zone to as low as  $10^\circ\text{C}$  in the coldest zone (Figure 6). The distribution pattern of these seasonal zones is rather different for the Ten, where a rather homogenous zone for inner land occurs during the winter season and partly extends into March (Figure 7). This pattern is decoupled into two major zones in April to June with a variable zonation pattern and returns to one major inner land zone from July to November. The extent of change in Ten varies from  $>30$  to  $<8^\circ\text{C}$ . In areas with high altitude (more than 1000 m) such as Jabal Jis, the average air temperature is generally below  $10^\circ\text{C}$  and occasionally may reach  $0^\circ\text{C}$  or less.

The general distribution of air temperatures in the UAE during the winter season nighttime (Ten) is  $10\text{--}15^\circ\text{C}$  in most areas, while it is at  $25\text{--}30^\circ\text{C}$  in the summer season (Figure 7). In all seasons other than the summer months, the air temperatures are moderate during nighttime ( $<25^\circ\text{C}$ ). There is a relatively low-temperature zone in the interior desert with temperatures of  $25\text{--}30^\circ\text{C}$  in summer and  $10\text{--}15^\circ\text{C}$  in winter. The air temperature during daytime and nighttime has the same spatial patterns across the UAE. Namely, during the daytime, the air temperature increases moving further away from the north and northwest and along the coastline to the south and southeast where the bar desert receives more solar radiation, which heats the ambient air. Air temperature in towns is higher than the surrounding region; this process is known as the Urban Heat Island (UHI), and at daytime, the inverse occurs, so it is called the Urban Cool Island (UCI), which may be essential for future research in the region.

To explore the difference between Ted and Ten patterns, we use the diurnal temperature range (DTR), which is an essential element for reflecting thermal environment

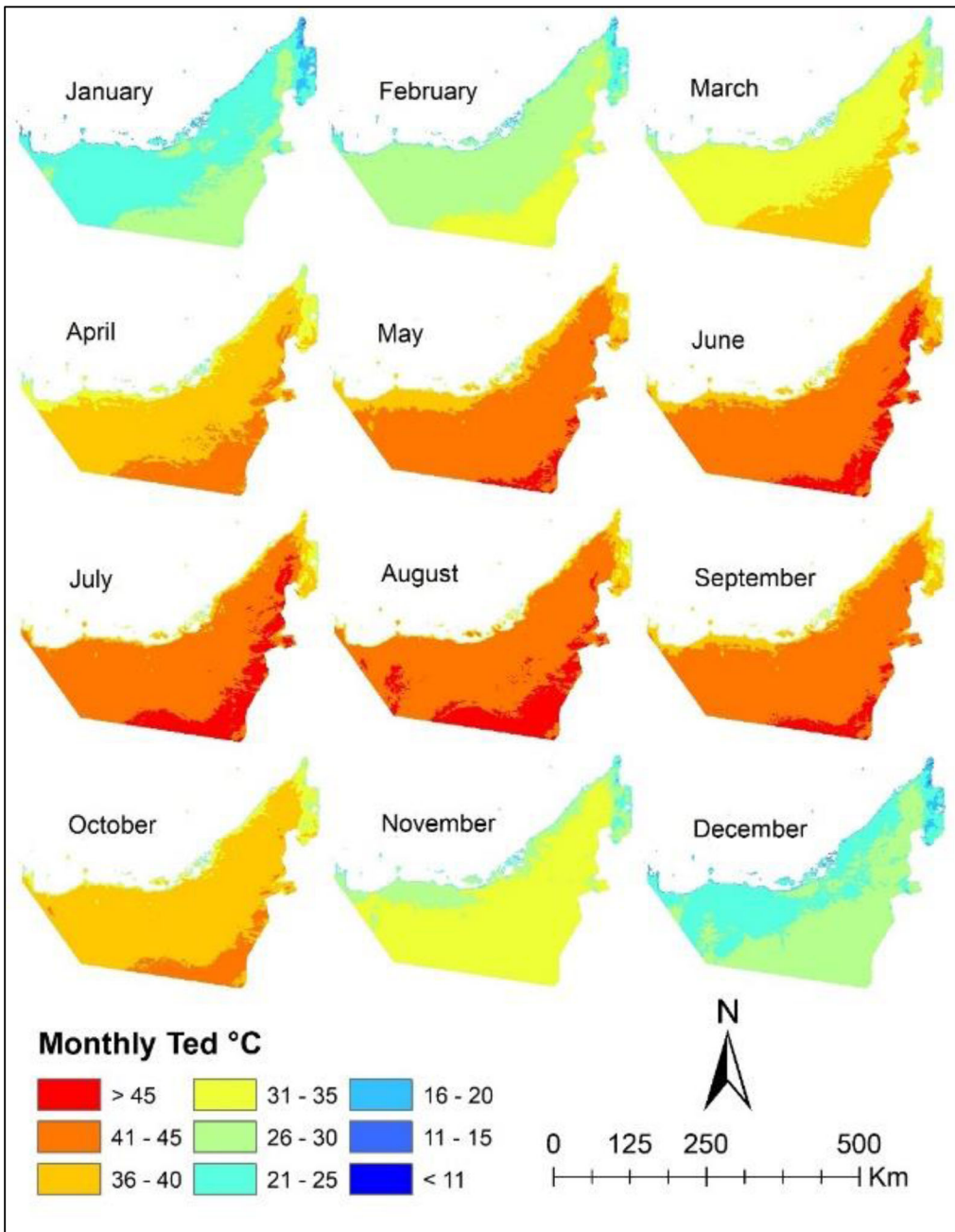


**Figure 6.** Spatial distribution of average monthly maximum air temperature (Ted) for UAE over the period 2003–2019.

analysis (Figure 8). The results reveal the persistence of four major Ted zones with temperature trends increasing from the coastal and mountain areas towards the inner land with a temperature span between 19 and 40 °C. Despite the fine temperature zonation given in Figure 8, the zonation can be generally grouped into two zones of 34–40 °C inner land zone and 19–34 °C coastal and mountain zone. The Ten mean annual zonation is

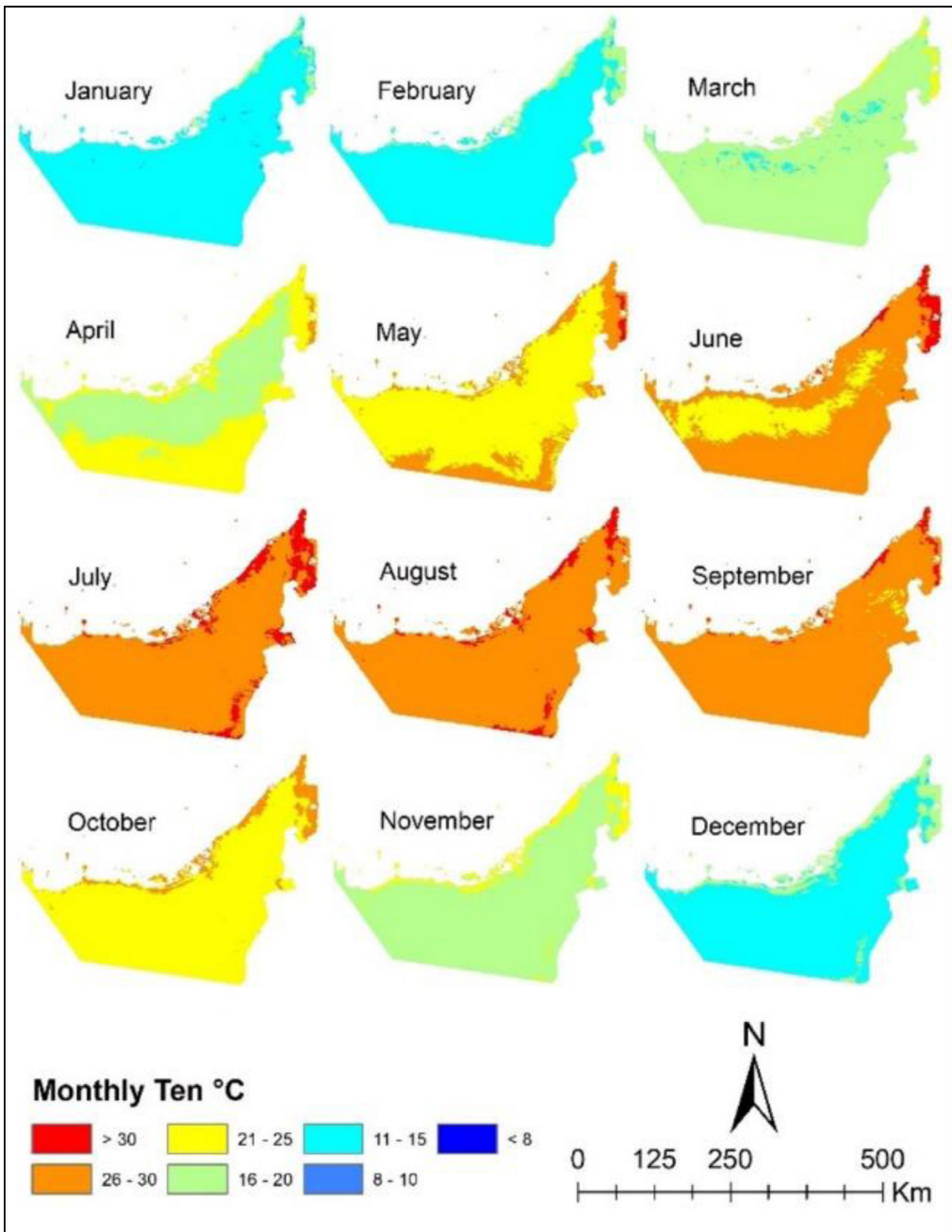


**Figure 7.** Spatial distribution of average monthly minimum air temperature (Ten) for the UAE over the period 2003–2019.

characterized by a major inner land zone with temperature below 22°C and a costal and mountain zone with a temperature between 23 and 27°C. The hotter Ted in mountain and coastal zones in comparison to Ten is due to the proximity to the sea and the higher elevations that leads to a temperate air temperature environment.

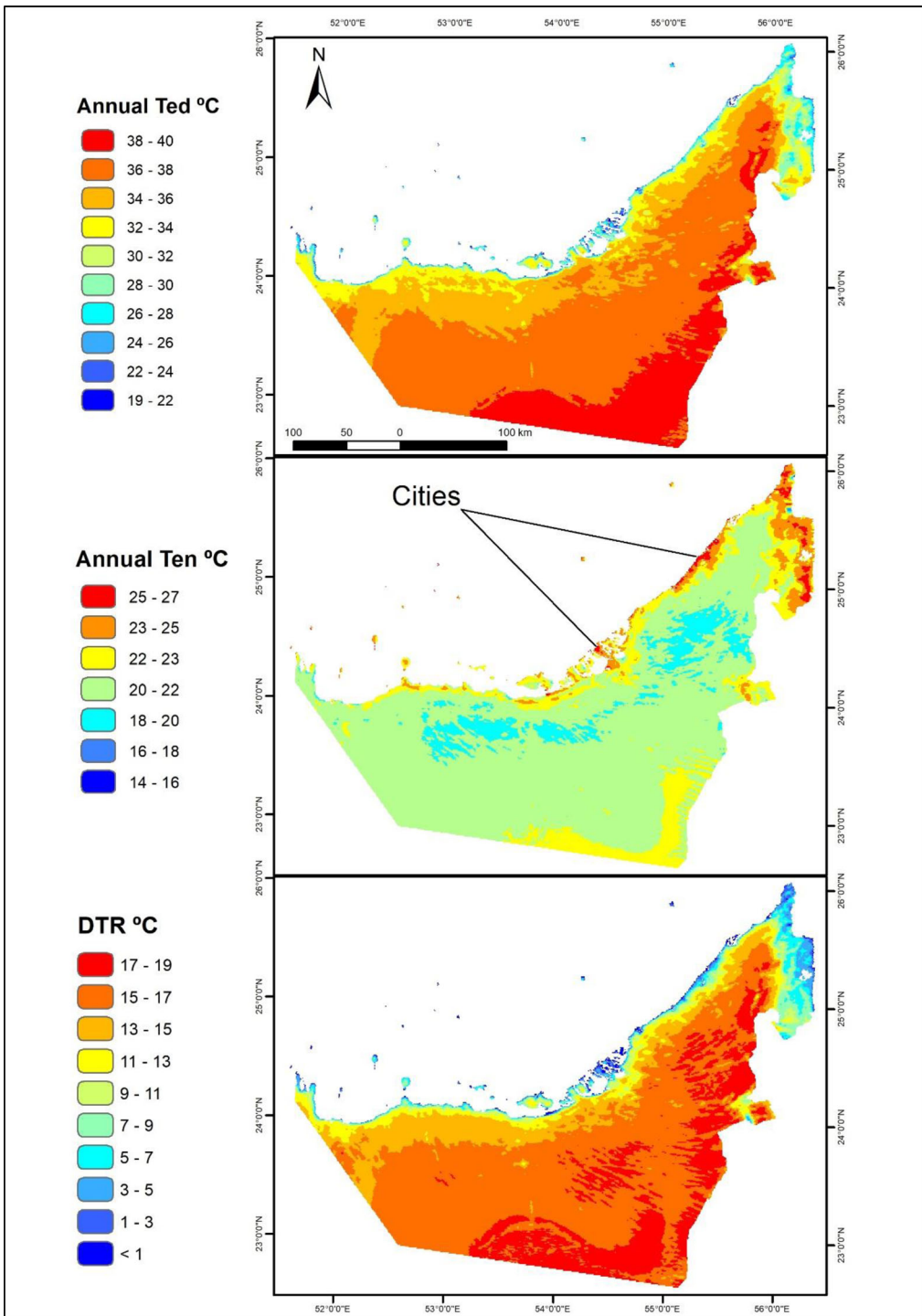


**Figure 8.** The annual mean maximum (Ted), minimum (Ten), and diurnal temperature range (DTR) of air temperature of the UAE for the period 2003–2019.



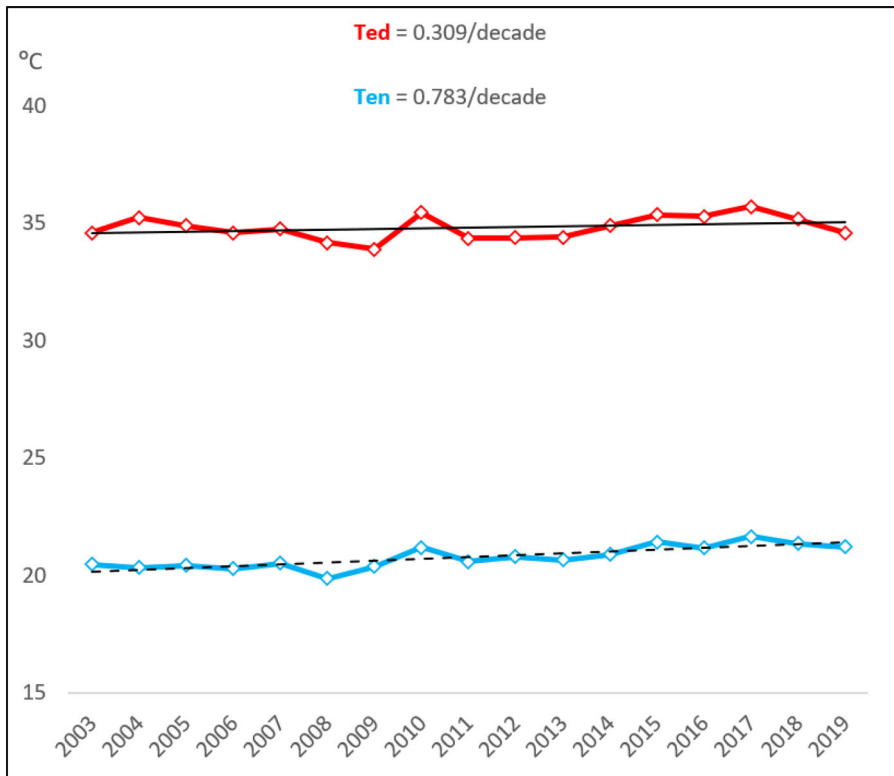


**Figure 9.** The mean annual (Ted, red line) and (Ten, blue line) for time series of the 11 weather stations used here in the period 2003–2019.

DTR is an essential element of the climate system and was used for urban thermal environment analysis, for example, extensive heat waves, heat-related health issues, landscaping and recreation, and engineering of heat transfer efficiency in buildings and roads (Duan et al. 2014; Wang and Upreti 2019; Yang et al. 2020; Chen et al. 2020). The pattern of DTR closely resembles the pattern of Ted, where the mountains and coastal zones indicate cooler temperatures than the inner land zones. The span of the DTR is between about 19 to  $<1^{\circ}\text{C}$ , with most of the areas with temperature below  $11^{\circ}\text{C}$  occurring in the mountain and coastal zones. It is important to mention that most of the large cities, e. g. Dubai, Abu Dhabi, and Sharjah, in the UAE, are also located along the coastal zone. The relatively small DTR along the coastal zones is likely the temperate thermal environment that is modulated by proximity to the sea as vegetation cover is rather scarce in the UAE. The relatively large DTR in the inner land (mainly covered by sand dunes) is that the ambient air warms slower, and the land surface warms faster in the day, and similarly, the surface cools faster in the night. Therefore, the desert reveals higher diurnal variation air temperature than the mountains and coastal regions (Figure 8).

The mean annual Ted and Ten in the studied period (2003–2019) reveals rather small variations with the Ted around  $35^{\circ}\text{C}$  and Ten around  $20^{\circ}\text{C}$  (Figure 9). There is, however, a slight increase in the trends from 2003 to 2019, with about  $0.31^{\circ}\text{C}$  and  $0.78^{\circ}\text{C}$  per decade, for the Ted and Ten, respectively. This temperature increase may not be uniform all over the UAE, as also evidenced by the spatial distribution patterns. The projection of these data for future predictions of climate change, and assuming constant decadal values, indicates that there will be a more rapid increase in the nighttime temperature compared

to the daytime. On average, there will be about a  $1 - 2^{\circ}\text{C}$  increase in the mean annual air temperature by the end of 2030, which is comparable to the estimate made by Murad and Aldahan (2019) for the period 1972–2020.

#### 4. Conclusion

In this paper, for the first time, we presented the estimation of monthly average maximum and minimum air temperature ( $T_{\text{ed}}$  and  $T_{\text{en}}$ ) over the UAE using Aqua MODIS LST data ( $LST_{\text{d}}$  and  $LST_{\text{n}}$ ) and measured air temperature ( $T_{\text{max}}$  and  $T_{\text{min}}$ ) observations from 11 weather stations from 2003 to 2019 by employing the linear regression method. The significant findings of this study show a strong correlation between these two datasets ( $R^2 > 0.94$ ) and a high accuracy achieved in the linear regression with minimal errors ( $RMSE < 2^{\circ}\text{C}$ ), which implies that the linear regression method provided a reasonable monthly air temperature maximum and minimum. Based on this result, MODIS Aqua LST products have been shown to be a reliable source for  $T_{\text{ed}}$  and  $T_{\text{en}}$ . The detailed  $1\text{ km}^2$  air temperature products (monthly air temperature maximum, minimum) as given by the linear regression can itself act as a meteorological station with confident and provide accurate records where each pixel represents the associated temperature.

Therefore, a remotely sensed dataset could be an alternative and surrogate to the ground meteorological stations, which then provide data with high resolution and extensive geographical coverage. For example, some areas in the UAE do not have any meteorological stations, however, this present investigation efficiently determined these locations' air temperature in a rigorous fashion. Specifically, in the Al Khazna area, which is about 45 km east of Al Wathbah (AW) ground meteorological station, the estimated maximum and minimum temperature for May was  $41.7^{\circ}\text{C}$  and  $23.5^{\circ}\text{C}$ , while the AW station records were  $41.8^{\circ}\text{C}$  and  $22.7^{\circ}\text{C}$  for the maximum and minimum air temperature in May, respectively.

This study is instrumental in the UAE or other neighbouring countries because the results have numerous applications in the fields of hydrological, agriculture, environmental, ecological, climate change, economic, and societal growth. As an example, for the construction of new urban communities and the latest reclamation projects in UAE's desert area, the selection of low diurnal temperature variation should be considered because it directly affects the quality of life and economic factors pertaining to living in these regions. Furthermore, time-series data can provide the potential for evaluation of anthropogenic activities' effect on climate change (such as urbanization, changes in land-use), at both the local and regional climate scale.

The limitation of the MODIS LST products in  $T_{\text{a}}$  estimation is that it works appropriately in clear-sky conditions as it retrieved data by using thermal infrared data. Moreover, the data of LST from MODIS starts from March 2000, restricting the prediction of  $T_{\text{a}}$  before that.

In future studies, specifically conducted on large areas with more varied and more complex land surface characteristics, other auxiliary variables should be considered that can reflect land surface characteristics and resulting temperature variations. UHI and UCI should be analyzed in further research. Due to rapidly advancing sensor technology, soon, the existing spatial resolution of 1 km will be more improved.

#### Disclosure statement

No potential conflict of interest was reported by the author(s).

## ORCID

Abduldaem S. Alqasemi  <http://orcid.org/0000-0002-1617-9469>  
 Mohamed E. Hereher  <http://orcid.org/0000-0003-4875-8286>  
 Ayad M. Fadhil Al-Quraishi  <http://orcid.org/0000-0001-7732-129X>  
 Hakim Saibi  <http://orcid.org/0000-0001-8803-6945>  
 Abdelgadir Abuelgasim  <http://orcid.org/0000-0001-8897-4181>

## References

- Barbulescu A, Nazzal Y. 2020. Statistical analysis of dust storms in the United Arab Emirates. *Atmos Res.* 231:104669. <https://doi.org/https://doi.org/10.1016/j.atmosres.2019.104669>.
- Benali A, Carvalho AC, Nunes JP, Carvalhais N, Santos A. 2012. Estimating air surface temperature in Portugal using MODIS LST data. *Remote Sens Environ.* 124:108–121.
- Chen G, Wang D, Wang Q, Li Y, Wang X, Hang J, Gao P, Ou C, Wang K. 2020. Scaled outdoor experimental studies of urban thermal environment in street canyon models with various aspect ratios and thermal storage. *Sci Total Environ.* 726:138147. <https://doi.org/https://doi.org/10.1016/j.scitotenv.2020.138147>.
- Chen Y, Sun H, Li J. 2016. Estimating daily maximum air temperature with MODIS data and a daytime temperature variation model in Beijing urban area. *Remote Sens Lett.* 7(9):865–874.
- Duan SB, Li ZL, Tang BH, Wu H, Tang R, Bi Y, Zhou G. 2014. Estimation of diurnal cycle of land surface temperature at high temporal and spatial resolution from clear-sky MODIS data. *Remote Sens.* 6(4):3247–3262.
- Duan SB, Li ZL, Wu H, Leng P, Gao M, Wang C. 2018. Radiance-based validation of land surface temperature products derived from Collection 6 MODIS thermal infrared data. *Int J Appl Earth Obs Geoinf.* 70:84–92.
- El Kenawy AM, Hereher ME, Robaa SM. 2019. An assessment of the accuracy of MODIS land surface temperature over Egypt using ground-based measurements. *Remote Sens.* 11(20):2369..
- El Kenawy AM, Lopez-Moreno JJ, McCabe MF, Robaa SM, Domínguez-Castro F, Peña-Gallardo M, Trigo RM, Hereher ME, Al-Awadhi T, Vicente-Serrano SM. 2019. Daily temperature extremes over Egypt: Spatial patterns, temporal trends, and driving forces. *Atmos Res.* 226:219–239.
- Fadhil AM. 2011. Drought mapping using Geoinformation technology for some sites in the Iraqi Kurdistan Region. *Int J Digital Earth.* 4(3):239–257.
- Hengl T, Heuvelink GBM, Tadić MP, Pebesma EJ. 2012. Spatio-temporal prediction of daily temperatures using time-series of MODIS LST images. *Theor Appl Climatol.* 107(1–2):265–277.
- Hereher ME. 2017. Effects of land use/cover change on regional land surface temperatures: severe warming from drying Toshka lakes, the Western Desert of Egypt. *Nat Hazards.* 88(3):1789–1803.
- Hereher ME. 2019. Estimation of monthly surface air temperatures from MODIS LST time series data: application to the deserts in the Sultanate of Oman. *Environ Monit Assess.* 191:9..
- Hereher ME, El Kenawy A. 2020. Extrapolation of daily air temperatures of Egypt from MODIS LST data. *Geocarto Int.*
- Huang R, Zhang C, Huang J, Zhu D, Wang L, Liu J. 2015. Mapping of daily mean air temperature in agricultural regions using daytime and nighttime land surface temperatures derived from TERRA and AQUA MODIS data. *Remote Sensing.* 7(7):8728–8756.
- IPCC. 2017. Meeting Report of the Intergovernmental Panel on Climate Change Expert Meeting on Mitigation, Sustainability and Climate Stabilization Scenarios [Shukla PR, Skea J, Diemen R, Huntley E, Pathak M, Portugal-Pereira J, Scull J, Slade R, eds.]. IPCC Working Group III Technical Support Unit, Imperial College London, London, UK, pp. 44.
- Janatian N, Sadeghi M, Sanaeinejad SH, Bakhshian E, Farid A, Hasheminia SM, Ghazanfari S. 2017. A statistical framework for estimating air temperature using MODIS land surface temperature data. *Int J Climatol.* 37(3):1181–1194.
- Jones P, Jedlovec G, Suggs R, Haines S. 2004. Using modis LST to estimate minimum air temperatures at night. Conference on Satellite Meteorology and Oceanography, January, pp. 457–462.
- Kloog I, Nordio F, Coull BA, Schwartz J. 2014. Predicting spatiotemporal mean air temperature using MODIS satellite surface temperature measurements across the Northeastern USA. *Remote Sens Environ.* 150:132–139.

- Lin X, Zhang W, Huang Y, Sun W, Han P, Yu L, Sun F. 2016. Empirical estimation of near-surface air temperature in China from MODIS LST data by considering physiographic features. *Remote Sens.* 8(8):629–615.
- Liu H, Zhou Q, Zhang S, Deng X. 2019. Estimation of summer air temperature over China using Himawari-8 AHI and numerical weather prediction data. *Adv Meteorol.* 2019:1–10.
- Meyer H, Katurji M, Detsch F, Morgan F, Nauss T, Roudier P, Zawar-Reza P. 2019. AntAir: satellite-derived 1 km daily Antarctic air temperatures since 2003. *Earth Syst Sci Data Discuss.* 2019:1–18.
- Misslin R, Vaguet Y, Vaguet A, Daudé É. 2018. Estimating air temperature using MODIS surface temperature images for assessing *Aedes aegypti* thermal niche in Bangkok, Thailand. *Environ Monit Assess.* 190:9..
- MODIS Web. (n.d.). [accessed 2020 January 7]. <https://modis.gsfc.nasa.gov/data/>.
- MODIS Land Team Home Page. (n.d.). [accessed 2020 January 14]. <https://modis-land.gsfc.nasa.gov/ValStatus.php?ProductID=MOD11>.
- Mostovoy GV, King RL, Reddy KR, Kakani VG, Filippova MG. 2006. Statistical estimation of daily maximum and minimum air temperatures from MODIS LST data over the State of Mississippi. *GISci Remote Sens.* 43(1):78–110.
- Murad A, Aldahan A. 2019. The impact of climate change on the future resources of the UAE. In *climate change and the future of water*. The Emirates Center for Strategic Studies and Research, pp. 45–69.
- Noi PT, Degener J, Kappas M. 2017. Comparison of multiple linear regression, cubist regression, and random forest algorithms to estimate daily air surface temperature from dynamic combinations of MODIS LST data. *Remote Sens.* 9(5):398..
- Noi PT, Kappas M, Degener J. 2016. Estimating daily maximum and minimum land air surface temperature using MODIS land surface temperature data and ground truth data in Northern Vietnam. *Remote Sensing.* 8(12):1002..
- Otgonbayar M, Atzberger C, Mattiuzzi M, Erdenedalai A. 2019. Estimation of climatologies of average monthly air temperature over mongolia using MODIS land surface temperature (LST) time series and machine learning techniques. *Remote Sens.* 11(21):1–24.
- Phan TN, Kappas M, Nguyen KT, Tran TP, Tran QV, Emam AR. 2019. Evaluation of MODIS land surface temperature products for daily air surface temperature estimation in northwest Vietnam. *Int J Remote Sens.* 40(14):5544–5562.
- Serra C, Lana X, Martínez MD, Roca J, Arellano B, Biere R, Moix M, Burgueño A. 2020. Air temperature in Barcelona metropolitan region from MODIS satellite and GIS data. *Theor Appl Climatol.* 139(1-2): 473–492.
- Shah DB, Pandya MR, Trivedi HJ, Jani AR. 2012. Estimation of minimum and maximum air temperature using MODIS data over Gujarat. *J Agrometeorol.* 14(2):111–118. <http://www.mosdac.gov.in>.
- Shah DB, Pandya MR, Trivedi HJ, Jani AR. 2013. Estimating minimum and maximum air temperature using MODIS data over Indo-Gangetic Plain. *J Earth Syst Sci.* 122(6):1593–1605.
- Singh S, Bhardwaj A, Singh A, Sam L, Shekhar M, Martín-Torres FJ, Zorzano MP. 2019. Quantifying the congruence between air and land surface temperatures for various climatic and elevation zones of Western Himalaya. *Remote Sens.* 11(24):2889..
- Stisen S, Sandholt I, Nørgaard A, Fensholt R, Eklundh L. 2007. Estimation of diurnal air temperature using MSG SEVIRI data in West Africa. *Remote Sens Environ.* 110(2):262–274.
- Vancutsem C, Ceccato P, Dinku T, Connor SJ. 2010. Evaluation of MODIS land surface temperature data to estimate air temperature in different ecosystems over Africa. *Remote Sens Environ.* 114(2):449–465.
- Vogt JV, Viau AA, Paquet F. 1997. Mapping regional air temperature fields using satellite-derived surface skin temperatures. *Int J Climatol.* 17(14):1559–1579.
- Wan Z. 2008. New refinements and validation of the MODIS Land-Surface Temperature/Emissivity products. *Remote Sens Environ.* 112(1):59–74.
- Wan Z. 2014. New refinements and validation of the collection-6 MODIS land-surface temperature/emissivity product. *Remote Sens Environ.* 140:36–45.
- Wan Z, Hook S, Hulley G. 2015. MYD11A2 MODIS/aqua land surface temperature/emissivity 8-day L3 global 1 km SIN grid V006. NASA EOSDIS Land Processes DAAC..
- Wan Z, Zhang Y, Zhang Q, Li Z. l. 2002. Validation of the land-surface temperature products retrieved from terra moderate resolution imaging spectroradiometer data. *Remote Sens Environ.* 83(1-2): 163–180.
- Wang W, Liang S, Meyers T. 2008. Validating MODIS land surface temperature products using long-term nighttime ground measurements. *Remote Sens Environ.* 112(3):623–635.

- Wang ZH, Upreti R. 2019. A scenario analysis of thermal environmental changes induced by urban growth in Colorado River Basin, USA. *Landscape Urban Plann.* 181:125–138. <https://doi.org/https://doi.org/10.1016/j.landurbplan.2018.10.002>.
- Xu Y, Qin Z, Shen Y. 2012. Study on the estimation of near-surface air temperature from MODIS data by statistical methods. *Int J Remote Sens.* 33(24):7629–7643.
- Yang YZ, Cai WH, Yang J. 2017. Evaluation of MODIS land surface temperature data to estimate near-surface air temperature in Northeast China. *Remote Sens.* 9(5):410–419.
- Yang Y, Zhang M, Li Q, Chen B, Gao Z, Ning G, Liu C, Li Y, Luo M. 2020. Modulations of surface thermal environment and agricultural activity on intraseasonal variations of summer diurnal temperature range in the Yangtze River Delta of China. *Sci Total Environ.* 736:139445. <https://doi.org/https://doi.org/10.1016/j.scitotenv.2020.139445>.
- Zhang W, Huang Y, Yu Y, Sun W. 2011. Empirical models for estimating daily maximum, minimum and mean air temperatures with MODIS land surface temperatures. *Int J Remote Sens.* 32(24):9415–9440.
- Zheng X, Zhu J, Yan Q. 2013. Monthly air temperatures over northern China estimated by integrating MODIS data with GIS techniques. *J Appl Meteorol Climatol.* 52(9):1987–2000.
- Zhou W, Peng B, Shi J, Wang T, Dhital YP, Yao R, Yu Y, Lei Z, Zhao R. 2017. Estimating high resolution daily air temperature based on remote sensing products and climate reanalysis datasets over glacierized basins: a case study in the Langtang Valley, Nepal. *Remote Sens.* 9(9):959..
- Zhu W, Lü A, Jia S. 2013. Estimation of daily maximum and minimum air temperature using MODIS land surface temperature products. *Remote Sens Environ.* 130:62–73.